Preparation, Structures, and Physical Properties of Tetrakis(alkylthio)tetraselenafulvalene (TTC_n-TSeF, $n = 1$–15)

Gunzi Saito,*[1,2,3] Yukihiro Yoshida,[1,2] Hidenobu Murofushi,[3,†] Naoko Iwasawa,[3,††] Takaaki Hiramatsu,[4,5] Akihiro Otsuka,[2,3,4] Hideki Yamochi,[2,3,4] Kimio Isa,[6] Eriko Mineo-Ota,[7] Michiko Konno,[7,†††] Takehiko Mori,[8,††††] Ken-ichi Imaeda,[8,†††††] and Hiroo Inokuchi[8,††††††]

[1]Research Institute, Meijo University, 1-501 Shiogamaguchi, Tempaku-ku, Nagoya 468-8502

[2]Division of Chemistry, Graduate School of Science, Kyoto University, Sakyo-ku, Kyoto 606-8502

[3]Institute for Solid State Physics, The University of Tokyo, Roppongi, Minato-ku, Tokyo 106

[4]Research Center for Low Temperature and Materials Sciences, Kyoto University, Sakyo-ku, Kyoto 606-8501

[5]Institute for Integrated Cell-Material Sciences, Kyoto University, Sakyo-ku, Kyoto 606-8501

[6]Faculty of Education and Regional Studies, University of Fukui, Bunkyo, Fukui 910-8507

[7]Department of Chemistry, Faculty of Science, Ochanomizu University, 2-1-1 Otsuka, Bunkyo-ku, Tokyo 112-8610

[8]Institute for Molecular Science, Myodaiji, Okazaki 444-8585

Received September 9, 2009; E-mail: gsaito@ccmfs.meijo-u.ac.jp

A series of tetrakis(alkylthio)tetraselenafulvalene compounds (TTC_n-TSeF, $n = 1$–15) were prepared by a one-step reaction between dialkyl disulfide and tetralithiated TSeF. Molecular properties (redox potentials and optical absorptions in solution) and solid-state properties (thermal behaviors, electric conductivities, and molecular and crystal structures for $n = 1$ and 10) were studied. TTC_n-TSeF compounds are weak electron donor molecules and characterized by small on-site Coulomb repulsion. TTC_1-TSeF has a high-dimensional conduction network owing to the presence of high-dimensional heteroatomic contacts, "Atomic-Wire Effect." The π-moieties of TTC_{10}-TSeF were fastened by the alkyl chains ("Fastener Effect") to form π-columns and there are a variety of short heteroatomic contacts resulting in two-dimensional electronic structure. Electrical conductivity exhibited peculiar enhancement for $n = 1$ and $7 \leq n \leq 14$ owing to the presence of high-dimensional conduction paths. These compounds may manifest high carrier mobility, and are good candidates for the field-effect transistor channel based on the advantageous features: low dark conductivity, low donor ability, on-site Coulomb repulsion energy, high-dimensional π-electron structure, and high solubility in organic solvents.

Some single-component organic compounds composed of neutral closed shell molecules have evoked highly conductive semiconductors with high carrier mobility and low solid-state ionization potentials, by making use of the "Fastener Effect"[1–13] and/or heteroatomic contacts.[14–18] In the "Fastener" molecules consisting of a central π-segment and peripheral long alkyl chains, intermolecular van der Waals interactions between the alkyl chains (paraffin part) assemble the π-segments to form π-column and further enhance the intermolecular interactions within the π-column, as schematically shown in Scheme 1.[1] This results in the formation of robust carrier paths for π-electrons embedded in paraffin and the compounds manifest intriguing behaviors in thermal, electronic, transport, and structural properties (Fastener Effect). We have reported these properties for the series of tetrakis(alkylchalcogeno)tetrachalcogenafulvalene: TYC_n-TXF, X is sulfur (X = T); Y is sulfur (Y = T), selenium (Y = Se), or tellurium (Y = Te); $n = 1$–18, Scheme 2).[1–11,19–28]

The n dependence of melting point (T_m) for TTC_n-TTF is seen in Figure 1.[20,23] The melting point decreased drastically with elongation of alkyl chains and showed a minimum at $n = 4$–6 depending on X and Y. At higher n, the Fastener Effect affords a gradual increase of melting point. The increased intermolecular interactions enhanced both electric conductivity up to 10^{-6} S cm^{-1} (TTC_{10}-TTF[1,3] and $TSeC_8$-TTF[7]) and bulk carrier mobility up to 6–20 cm^2 V^{-1} s^{-1} (TTC_n-TTF, $n = 8$ and 10, time of flight (TOF) method).[9] At low n region of TYC_n-TTF having bulkier Y, i.e., $TTeC_1$-TTF,[4] the presence of three-dimensional heteroatomic contacts connecting the π-moieties enhanced the electric conductivity up to 10^{-5} S cm^{-1} and bulk

† Present address: New Business Development & Promotion Center, Asahi Glass Co., LTD
†† Present address: Department of Applied Chemistry, Faculty of Science and Technology, Keio University
††† Present address: Department of Chemistry and Biochemistry, Graduate School of Humanities and Sciences, Ochanomizu University
†††† Present address: Department of Chemistry and Materials Science, Tokyo Institute of Technology
††††† Present address: Department of Applied Chemistry, College of Engineering, Chubu University
†††††† Present address: Japan Aerospace Exploration Agency

Published on the web March 26, 2010; doi:10.1246/bcsj.20090240

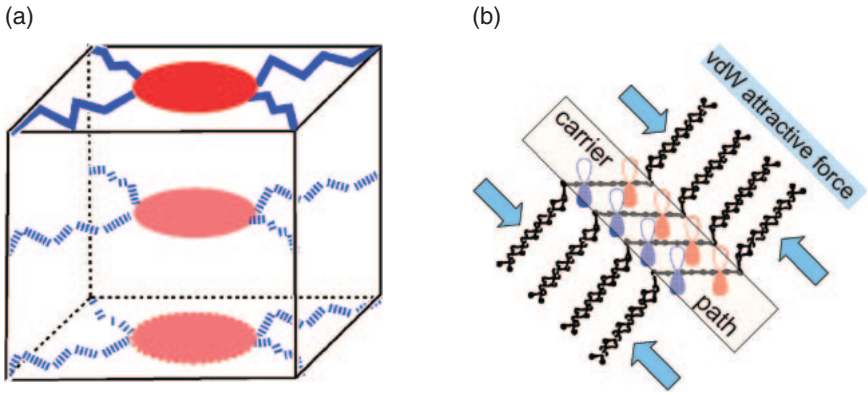

Scheme 1. (a) Schematic view of the Fastener Effect. The van der Waals attractive intermolecular interactions between alkyl chains (blue) enforce central π-segments (red) to form a column with small interplanar distance. (b) Molecular packing of chair-shaped TTC$_9$-TTF molecules,[19] where flat central C_6S_8 π-segments form carrier path by the aid of van der Waals attractive force of alkyl chains along the blue arrows.

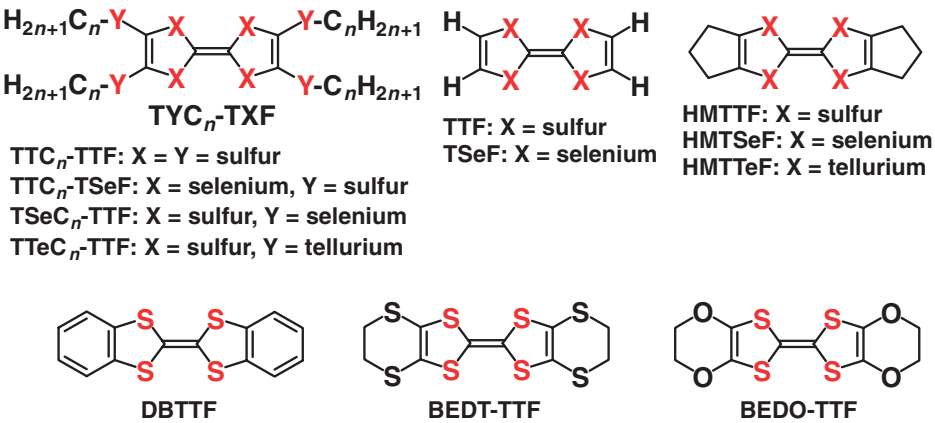

Scheme 2. Main molecules in text.

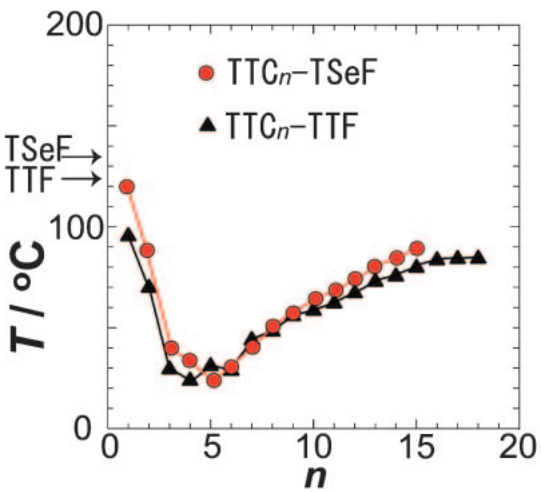

Figure 1. Melting points of TTC$_n$-TSeF are compared with those of TTC$_n$-TTF.[20,23] Minimum T_m's are 24.6 °C at $n = 4$ for TTC$_n$-TTF and 22.9 °C at $n = 5$ for TTC$_n$-TSeF.

carrier mobility up to 30 cm^2 V^{-1} s^{-1} ($\mu_h = 29$ and $\mu_e = 19$ cm^2 V^{-1} s^{-1} for TTeC$_1$-TTF).[4] Atomic-Wire Effect is a concept to represent this kind of enhancement of three-dimensional intermolecular interactions by heteroatomic contacts.[4,29] Here we show an extension of our work to a series of TTC$_n$-TSeF compounds concerning preparation, and thermal, physical, and structural properties, and discuss in comparison with those of TYC$_n$-TTF compounds. We will emphasize that the increase in size of the inner five-membered ring from TTF to TSeF has enhanced the electronic dimensionality of the semiconductor and thus TTC$_n$-TSeF is anticipated to be a good candidate for the field-effect transistor (FET) channel materials.

Experimental

Optical measurements were carried out on a Perkin-Elmer 1600 Series FT-IR spectrometer (400–4000 cm^{-1}, resolution 4 cm^{-1}) for IR and near-IR regions, and on a Shimadzu UV-3100 spectrometer for visible and ultraviolet (300–800 nm, UV–vis–NIR) regions. DC conductivities of single crystals were measured between RT and T_m by standard two-probe method using gold wires of 10 μm in diameter with gold paste (Tokuriki, 8560-1A). Melting points were determined using a Yanaco MP-500D micro melting point apparatus. Differential scanning calorimetry (DSC) thermograms were measured on a Shimadzu DSC-60 instrument equipped with nitrogen cryostatic cooling. The samples were heated up to 150 °C for TTC$_1$-TSeF and 100 °C for TTC$_{10}$-TSeF (1st heating in Figure 3), and then cooled down to −120 °C at a rate of −25 °C min^{-1}. After standing for 10 min, they were heated at a rate of 10 °C min^{-1} (2nd heating in Figure 3). While crystallization (T_c), solid–solid transition (T_s), and T_m were taken as onset of peaks, glass transition temperature (T_g) was taken as an onset of a heat

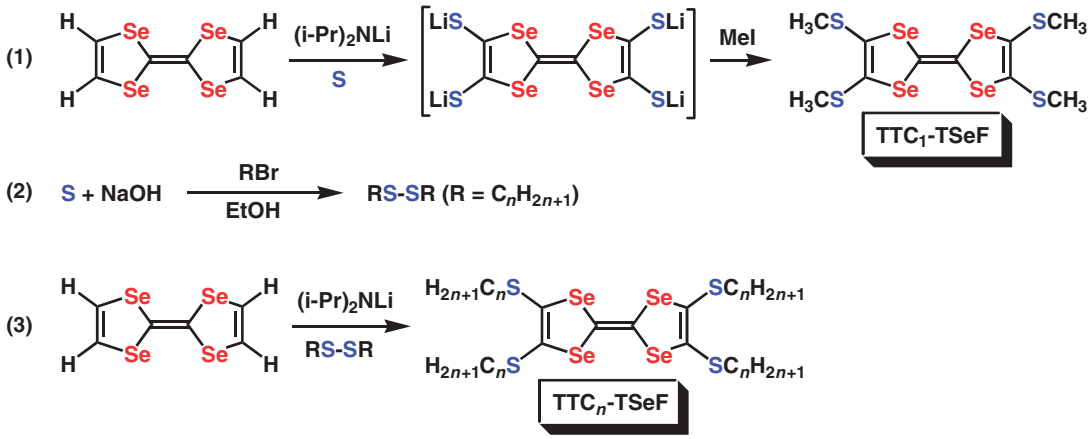

Scheme 3. Synthetic procedures of (1) TTC_1-TSeF by a two-step method, (2) dialkyl disulfides, and (3) TTC_n-TSeF by a one-step method.

capacity change. The temperature was calibrated by water and indium. Redox potentials were measured with supporting electrolyte of 0.1 M tetrabutylammonium tetrafluoroborate ((TBA)BF_4) in 1,2-dichloroethane using Pt electrode vs. saturated calomel electrode (SCE) at 22 °C. ^{1}H NMR measurements were conducted on a JEOL JNM-PMX60SI spectrometer operating at 60 MHz. The mass spectra were obtained with a JEOL-O1SG-2 double focusing mass spectrometer. Elemental analyses (C, H, N, S, Se, and halogen) were carried out by the Microanalytical Laboratory, Division of Chemistry, Graduate School of Science, The University of Tokyo.

X-ray diffraction data for TTC_n-TSeF ($n = 1$ and 10) were collected on a CCD diffractometer (Bruker SMART APEX II) with graphite monochromated Mo Kα radiation at room temperature (RT). The absorption correction was carried out using the program SADABS[30] in Bruker APEX2 software by a numerical method taking the crystal shape into consideration. The crystal structures were solved by a direct method of SHELXS[31] and refined by a full matrix least-squares method of F^2 by means of SHELXL.[32] The positional parameters of hydrogen atoms were calculated under a fixed C–H bond length of 0.96 Å for methyl groups and 0.97 Å for methylene groups with sp^3 configuration of the bonding carbon atoms. Crystallographic data have been deposited with Cambridge Crystallographic Data Centre: Deposition numbers CCDC-746300 for TTC_1-TSeF and CCDC-746301 for TTC_{10}-TSeF. Copies of the data can be obtained free of charge via http://www.ccdc.cam.ac.uk/conts/retrieving.html (or from the Cambridge Crystallographic Data Centre, 12, Union Road, Cambridge, CB2 1EZ, U.K.; Fax: +44 1223 336033; e-mail: deposit@ccdc.cam.ac.uk).

The intermolecular overlap integrals (S) were calculated by means of extended Hückel tight binding method with single-ζ parameters[33] on the basis of the crystal structures. The 3d-orbitals of the sulfur and selenium atoms were included in the calculation.

Results and Discussion

Synthesis. Among the TYC_n-TSeF series, $TSeC_1$-TSeF had been synthesized by the electrochemical reduction of CSe_2, however the synthetic procedure is tedious with poor yield[34] and cannot be applied to a series of TYC_n-TSeF. In the previous papers,[22,28] we have noticed that the introduction of outer methylthio groups to tetralithiated TSeF, which was prepared by lithiation with lithium diisopropylamide for 1–2 h at 0 °C, by a two-step method (Procedure 1 in Scheme 3) was hampered by the formation of undesired and intractable by-products. On the other hand, the direct and one-step introduction by dialkyl disulfide (Procedure 3 in Scheme 3) profoundly improved the reaction and afforded TTC_n-TSeF ($n \leq 15$, Supporting Information S1), where several dialkyl disulfides (RSSR, R = C_nH_{2n+1}, n = 1–5, 7, and 10) were purchased and other disulfides were synthesized (Procedure 2 in Scheme 3, Supporting Information S2).[35] The synthesized materials after purification were characterized by elemental analysis, and NMR, UV–vis, and mass spectra.

For TTC_{12}-TSeF, elements except S and N are far from the calculated values (Found: C, 53.62; H, 8.11; N, 0.00; S, 10.70; Se, 27.81%. Calcd: C, 54.34; H, 8.45; N, 0.00; S, 10.75; Se, 26.46%) indicating the material is not purified enough and the data for TTC_{12}-TSeF in the text may include some uncertainty. The same feature was seen for $n = 15$; the elemental analysis indicates that the product has an excess of selenium (Found: C, 57.97; H, 8.96; N, 0.00; S, 9.44; Se, 24.00%. Calcd: C, 58.21; H, 9.18; N, 0.00; S, 9.42; Se, 23.19%). The color, shape, yield, and T_m of the TTC_n-TSeF (n = 1–15) are summarized in Table 1.

For n = 16–18 the products contained almost no TSeF skeleton as indicated by the extremely low Se contents in the elemental analysis (Found: less than 4%, Calcd: more than 20%, Table S1). We will not discuss the compounds for $n \geq 16$.

Molecular Properties. Redox Potentials: As for the ionization potentials of the isolated TYC_n-TTF molecules, ultraviolet photoelectron spectroscopy in gas phase[2,5] and redox potentials in solution[21,22,36] have been so far elucidated and the latter is much conventional though the data includes ambiguity caused by the solvation term. The first and second redox potentials ($E^1_{1/2}$ and $E^2_{1/2}$) and the difference between them (ΔE), which is a measure of the on-site Coulomb repulsive energy of a molecule, of TTC_n-TSeF are summarized in Table 1. Similar to the series of TYC_n-TTF compounds,[21,22,36] the redox data for TTC_n-TSeF are insensitive to the length of the alkyl chains; $E^1_{1/2} = 0.79 \pm 0.01$ V, $E^2_{1/2} = 1.07 \pm 0.02$ V, $\Delta E = 0.28 \pm 0.02$ V (Figure 2). It has been known that the replacement of chalcogen atoms X in the TXF skeleton in the order from S to Se or Te stabilizes the HOMO level and gives rise to the increase of $E^1_{1/2}$, that corresponds to

Table 1. Characteristics of TTC$_n$-TSeF

n	Color, shape	Yield[a]/%	T_m[b]/°C	Redox potential[c]		
				$E^1_{1/2}$/V	$E^2_{1/2}$/V	ΔE/V
1	orange, needle	84.2	119.0–119.7	+0.78	+1.07	0.29
2	purple, thin plate	71.0	86.5–87.5	+0.79	+1.08	0.29
3	red, plate	74.6	39.7–40.2	+0.79	+1.08	0.29
4	red, needle	75.7	34.2–35.0	+0.78	+1.05	0.27
5	red, needle	32.5	22.9	+0.78	+1.06	0.28
6	red, needle	41.7	30.7–31.6	+0.78	+1.07	0.29
7	red brown, needle	74.2	37.2–37.8	+0.78	+1.08	0.30
8	red brown, plate	33.2	46.5–47.5	+0.78	+1.07	0.29
9	red brown, thin plate	54.8	55.7–56.5	+0.78	+1.05	0.27
10	red brown, plate	50.1	64.0–65.0	+0.79	+1.07	0.28
11	red brown, thin plate	65.1	68.3–69.2	+0.78	+1.05	0.27
12	red brown, powder	—	74.2–75.2	+0.78	+1.05	0.27
13	brownish green, powder	45.2	79.5–80.2	+0.80	+1.06	0.26
14	brownish green, powder	58.3	83.5–84.2	+0.80	+1.06	0.26
15	brown, powder	—	87.0–87.8	+0.80	+1.06	0.26

a) —: The yield of pure product could not be determined (see text). b) T_m (TSeF) = 135 °C. c) 0.1 M (TBA)BF_4 in 1,2-dichloroethane, Pt, vs. SCE, 22 °C.

the decrease of donor ability.[37] Accordingly, the $E^1_{1/2}$ values of TTC$_n$-TSeF are higher by 0.15 V than those of TTC$_n$-TTF (0.64 V). The donor ability of TTC$_n$-TSeF is a little weaker than that of weak TTF analog DBTTF ($E^1_{1/2}$ = 0.74 V). The addition of the four alkylthio groups to TSeF skeleton changed the $E^1_{1/2}$ value from 0.59 V (TSeF) to 0.79 V (TTC$_n$-TSeF) that corresponds to the weakened donor ability by 0.20 V.

The most interesting point is that ΔE (0.28 V) of TTC$_n$-TSeF is smaller than those of TYC$_n$-TTF (0.30–0.40 V) and is comparable to that of HMTTeF (0.28 V), indicating very weak on-site Coulomb repulsion. This feature stems from multiple reasons. The C_6X_4 π-moiety expands the own size in the order of S → Se → Te, which causes a decrease of ΔE in TSeF compounds compared with those of TTF compounds. Furthermore, the increased atomic electronegativity of outer chalcogen atom Y, which increases in the order of Te(2.1) → Se(2.4) → S(2.5), results in the decreased π-electron density on the central C_6X_4 moiety giving rise to a decrease of the on-site Coulomb repulsive energy in the order of TTeC$_n$-TXF → TSeC$_n$-TXF → TTC$_n$-TXF as well as the decrease of the donor ability in the same order.

Absorption Spectra: The absorption spectra of TTC$_n$-TSeF in chloroform are composed of three absorption bands λ_1 = 311–314 nm ($\log\varepsilon$ = 4.19–4.23), λ_2 = 376–383 nm ($\log\varepsilon$ = 3.55–3.58), and λ_3 = 477–507 nm ($\log\varepsilon$ = 2.28–2.81) (see Supporting Information, Table S2), similar to that observed for TSeF (293 (4.10), 368 (3.21), and 486 (2.12)). No obvious dependence on the length of the alkyl chains was observed concerning the absorption peaks and extinction coefficients. The absorption band λ_3 originates from the HOMO–LUMO transition and is known to appear very weakly for TXF compounds.[38] This band extends to longer wavelength for TTC$_n$-TSeF compared to those of conventional TTF compounds (433–459 nm for DBTTF, BEDT-TTF, and TTF in chloroform, and 483 nm for TTC$_{10}$-TTF in hexane) and is close to that of BEDO-TTF (518 nm). The threshold of the absorption band is around 650 nm (1.9 eV).

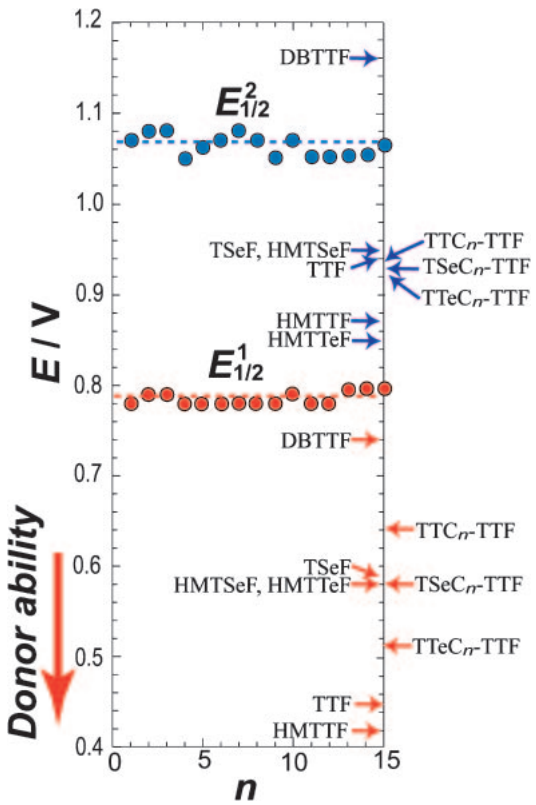

Figure 2. Redox potentials (0.1 M (TBA)BF_4 in 1,2-dichloroethane, Pt, vs. SCE, 22 °C) of TTC$_n$-TSeF are compared with those of TTF and its analogs (see Supporting Information, Table S3). Red circles and arrows: $E^1_{1/2}$, blue circles and arrows: $E^2_{1/2}$.

Solid-State Properties. Melting Point: Similarly to those observed in the series of TYC$_n$-TTF compounds,[20–24] the melting point (Table 1) was decreased drastically by the addition of alkylchalcogeno groups to TSeF (T_m = 135 °C). The T_m shows a minimum at n = 5 (T_m = 22.9 °C) and

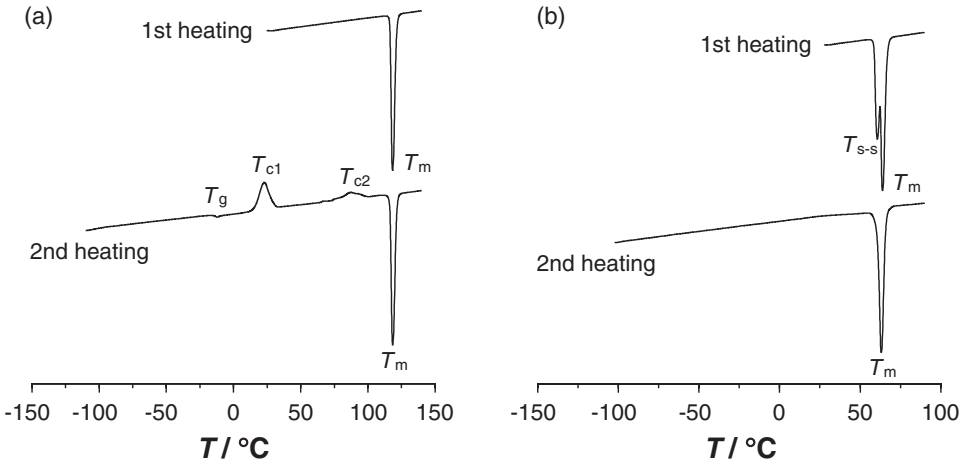

Figure 3. DSC charts for (a) TTC_1-TSeF and (b) TTC_{10}-TSeF.

increases gradually for $n \geq 5$ suggesting that the Fastener Effect operates in this n region. It is interesting to note that TTC_n-TSeF ($n = 5$ and 6) shows T_m below 32 °C similarly to $TSeC_n$-TTF ($n = 5$ and 6): they are liquid electron donors near RT with molecular weight >800. As is compared with that of TTC_n-TTF in Figure 1, the even–odd effect is not so obvious for TTC_n-TSeF.

The TTC_n-TTF compounds with small n (≤ 7) were characterized by the presence of the glassy state[23] where the glass temperatures very roughly follow the so called "2/3 law ($T_g/T_m \approx 2/3$)."[39] The glassy state was also observed for $TSeC_n$-TTF with $n \leq 7$, though T_g was not able to be defined due to the gradual transition.[7] On the other hand, the TYC_n-TTF (Y = T and Se) compounds with long alkyl chains exhibited solid–solid transition near T_m ($n \geq 8$ for Y = T, $n = 6$ and ≥ 9 for Y = Se)[7,23] and, in general, low-temperature phase (Phase I) exhibited higher conductivity than that of the high-temperature phase (Phase II).[7,9–11] For example, Phase I of TTC_8-TTF has lower RT resistivity (ρ_{RT}) and higher TOF mobility (μ_{TOF}) ($\rho_{RT} = 1.2 \times 10^5\,\Omega\,cm$, $\mu_{TOF} = 6.4$ $cm^2\,V^{-1}\,s^{-1}$) in comparison with Phase II ($\rho_{RT} = 7.0 \times 10^7$ $\Omega\,cm$, $\mu_{TOF} = 0.77\,cm^2\,V^{-1}\,s^{-1}$).[9,10] These two phases have very similar intra-column overlap patterns (as depicted in Figure 6c for TTC_{10}-TSeF) but a slightly different intra-column overlap integrals: $S = -4.89 \times 10^{-3}$ (I-Phase) and -3.66×10^{-3} (II-Phase). It is important to note that only a 1.3-fold increase in calculated overlap integrals corresponds to the enhancement both in carrier mobility by one order of magnitude and in electric conductivity by two orders of magnitude.

Figure 3 shows the DSC chart of TTC_n-TSeF ($n = 1$ and 10). In accordance with the thermal properties for TYC_n-TTF compounds,[22,27] a glassy state was observed for TTC_1-TSeF ($T_g = -15.6$ °C) but not for TTC_{10}-TSeF, while a solid–solid transition was observed for TTC_{10}-TSeF ($T_s = 58.2$ °C) but not for TTC_1-TSeF. The ratio T_g/T_m of TTC_1-TSeF is nearly 2/3. TTC_1-TSeF also exhibited two crystallization transitions ($T_c =$ 15.3 and 78 °C) similarly to those for TTC_n-TTF ($n \leq 7$).[23]

Resistivity: The RT resistivity and activation energy for conduction (ε_a) of TTC_n-TSeF without heat treatment are summarized in Table 2. Since not all TTC_n-TSeF afforded single crystals, the table includes the data on compressed pellet samples. TTC_5-TSeF was not measured since the compound easily liquefied.

It is interesting to note that the conductivity of TTC_n-TSeF with large n (10^7–$10^8\,\Omega\,cm$ on a single crystal for $n = 7$, 8, and 10) was considerably low in comparison with the TYC_n-TTF series; 10^5–$10^7\,\Omega\,cm$ for TTC_n-TTF, $10^6\,\Omega\,cm$ for $TSeC_n$-TTF and $TTeC_n$-TTF.[3,4,7]

For the series of TYC_n-TTF (Y = T and Se), the conductivity enhancement by taking the most resistive one as a standard is a good indicator to estimate the extra intermolecular interactions (right two columns in Table 2), though strictly speaking the comparison should be done concerning the anisotropic conducting behaviors measured on single crystals. For TTC_n-TTF, the conductivity enhancement for $n \geq 4$ clearly indicates the presence of the Fastener Effect. The most resistive compound among TTC_n-TSeF measured is TTC_4-TSeF on the compaction pellet ($\rho_{RT} = 1.0 \times 10^{14}\,\Omega\,cm$). The most conductive one (TTC_{10}-TSeF $\rho_{RT} = 1.5 \times 10^7\,\Omega\,cm$ on single crystal) reaches ca. 6.7×10^6 times the conductivity of $n = 4$. TTC_n-TSeF compounds with $n = 7$ and 8 on single crystals and $n = 9$, 11, and 13 on compressed pellets also exhibit large enhancement of 4.8×10^4–7.7×10^5 suggesting the Fastener Effect is active for $n \geq 7$. The significant decrease of activation energy for $n = 7$, 8, and 10 compared with those for $n = 1$ and 3 is in accordance with the manifestation of the Fastener Effect. These compounds are demonstrated by yellow shadow in Table 2.

As for TTC_1-TSeF, the large enhancement (7.7×10^4) is ascribed not to the Fastener Effect but to a formation of network of atomic contacts (Atomic-Wire Effect) in the crystal (vide infra), like those of $TSeC_1$-TTF (Phase I)[11] and $TTeC_1$-TTF.[4] Those are indicated by blue shadow in Table 2.

Molecular and Crystal Structures: Although the structure assuming the space group $P2_1/n$ had been reported for TTC_1-TSeF previously,[28] the better quality of diffraction data collected on a CCD diffractometer proved that the previous structure was incorrect. The following subsection concerns the correct structure with the space gorup $P2_1/c$. The crystal data for $n = 1$ and 10 are summarized in Table 3 and Supporting Information.

Table 2. Semiconductive Parameters and Conductivity Enhancement of TTC_n-TSeF Compared with Those of TTC_n-TTF and $TSeC_n$-TTF Compounds[a),b)]

n	TTC_n-TSeF			TTC_n-TTF	$TSeC_n$-TTF
	ρ_{RT}/Ω cm	ε_a/eV	$\rho_{RT}(n=4)/\rho_{RT}$	$\rho_{RT}(n=1)/\rho_{RT}$	$\rho_{RT}(n=4)/\rho_{RT}$
1	1.3×10^9	0.60	7.7×10^4	1 (Phase I)	2.2×10^5 (Phase I) 3.0×10^2 (Phase II)
2	1.0×10^{12} d)	—	1.0×10^2	2	6.7 × 10
3	2.6×10^{13}	0.86	4	3.0 × 10	3.3×10^2
4	1.0×10^{14} d)	—	1	4.7×10^3	1
5	—d)	—	—	4.5×10^2	6.3 × 10
6	3.6×10^{12} d)	—	2.8 × 10	7.6×10^2	1.7×10^5
7	1.3×10^8	0.18	7.7×10^5	1.2×10^3 (Phase I) 7.6×10^2 (Phase II)	2.3×10^4
8	1.7×10^8	0.20	5.9×10^5	2.4×10^4 (Phase I) 4.1×10^2 (Phase II)	2.9×10^5
9	1.7×10^{9} d)	—	5.9×10^4	8.3×10^3 (Phase I) 5.8×10^2 (Phase II)	2.7×10^5 d)
10	1.5×10^7	0.17	6.7×10^6	7.8×10^4	2.2×10^4 d)
11	2.1×10^9 d)	—	4.8×10^4	5.2×10^4	2.6×10^4 d)
12c)	5.9×10^{10} d)	—	1.7×10^3	5.5×10^2 d)	5.9×10^4 d)
13	1.7×10^9 d)	—	5.9×10^4	1.3×10^2 d)	3.9×10^4 d)
14	5.3×10^{10} d)	—	1.9×10^3	3.7×10^2 d)	3.4×10^4 d)
15	—	—	—	1.0×10^4 d)	6.7×10^4 d)

a) The yellow and blue shadows indicate the data on which Fastener Effect and Atomic-Wire Effect are regarded effective, respectively. b) —: Not measured. c) Data may be not intrinsic since the sample is impure. d) Compaction pellet sample.

Table 3. Crystallographic Data of TTC_1-TSeF and TTC_{10}-TSeF

	TTC_1-TSeF	TTC_{10}-TSeF
Formula	$C_{10}H_{12}S_4Se_4$	$C_{46}H_{84}S_4Se_4$
Formula weight	576.28	1081.25
Crystal system	Monoclinic	Triclinic
Space group	$P2_1/c$	$P\bar{1}$
Crystal size/mm^3	0.58 × 0.50 × 0.06	0.48 × 0.29 × 0.21
a/Å	9.1110(9)	7.9573(6)
b/Å	8.0115(8)	33.411(3)
c/Å	24.092(2)	5.1050(4)
α/°	90	93.111(1)
β/°	95.135(1)	102.373(1)
γ/°	90	88.452(1)
V/Å^3	1751.5(3)	1323.6(2)
Z	4	1
d_{calcd}/g cm^{-3}	2.185	1.356
Radiation	Mo Kα	Mo Kα
μ(Mo Kα)/cm^{-1}	88.36	29.58
Independent obsd reflections	4329	6341
Reflections with $I > 2\sigma(I)$	3334	5170
Refined parameters	168	247
$wR2$ (for all data)	0.0874	0.0804
R_{gt} (for $I > 2\sigma(I)$)	0.0363	0.0263
GOF	1.027	1.109

TTC_1-TSeF; Similarly to the TYC_n-TTF molecules with small n (e.g., TTC_n-TTF: $n = 1$ (Phase I),[40] 2,[41] 3;[25] $TSeC_2$-TTF[6]), TTC_1-TSeF forms a boat shape (Figure 4) in which

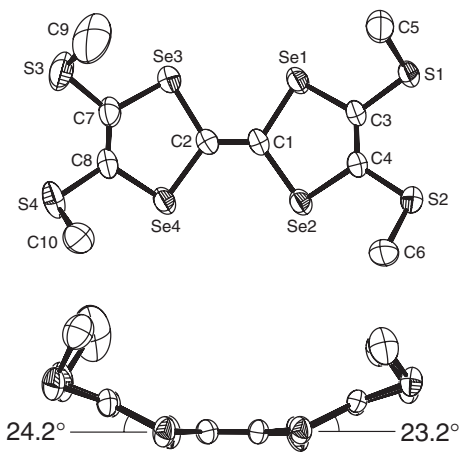

Figure 4. Molecular structure of TTC_1-TSeF showing the atom labeling scheme. Hydrogen atoms are omitted for clarity.

the π-segment is deformed like a boat and four alkyl chains stretch in the same side. The crystal structure of TTC_1-TSeF is isomorphous with Phase I of TTC_1-TTF.[40] The bending angles of 23.2 and 24.2° are similar to those of TTC_1-TTF (Phase I, 19.3 and 23.7°). One molecule is crystallographically unique. The two molecules A and B arrange almost orthogonally (Figure 5a) with the distance between the centers of them 5.33 Å (5.23 Å for TTC_1-TTF). Se atoms in the TSeF skeleton form short Se···Se atomic contacts less than the sum of the van der Waals radii (3.72–3.79 Å vs. van der Waals sum of 3.80 Å[42]) and a little longer Se···C atomic contacts (3.62–3.67 Å vs. 3.60 Å) as represented by dotted lines in Figure 5b. Outer sulfur atoms contribute to the formation of S···S atomic contacts

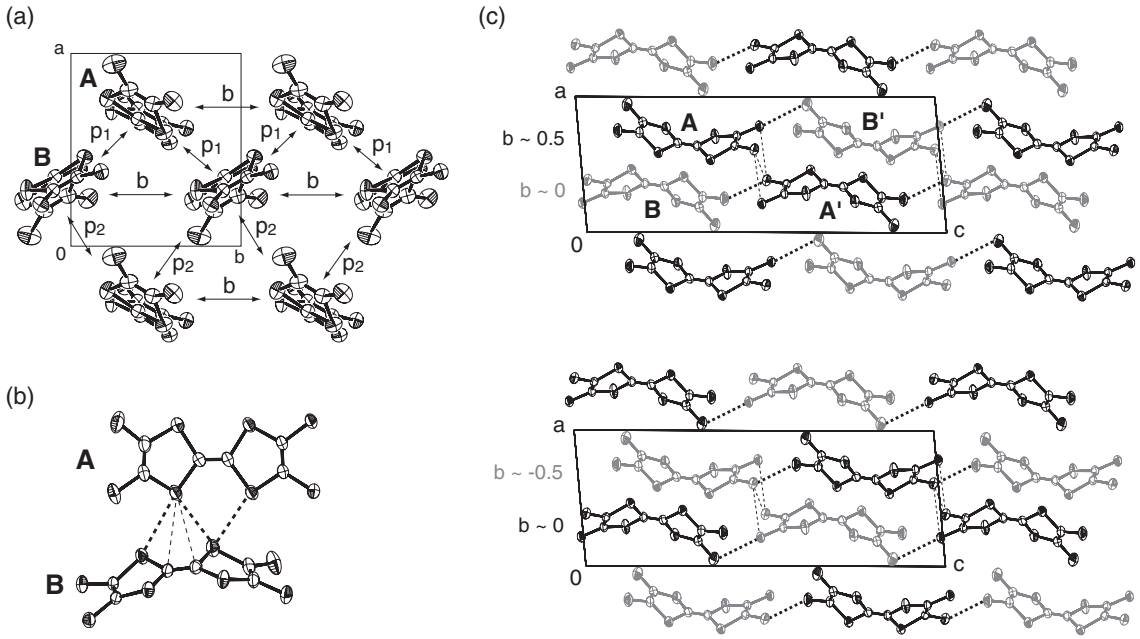

Figure 5. Crystal structures of TTC_1-TSeF, in which methyl groups are omitted for clarity. (a) Viewed along the c axis with scheme of the intermolecular overlap integrals. $b = 1.8 \times 10^{-3}$, $p_1 = 16.0 \times 10^{-3}$, $p_2 = -0.66 \times 10^{-3}$. (b) Intermolecular short atomic contacts between A and B molecules. Thick and thin dotted lines indicate the Se···Se and Se···C contacts, respectively. (c) Viewed along the b axis, in which only molecules located at $0 < b < 0.5$ (upper figure) and $-0.5 < b < 0$ (lower figure) are depicted. Gray and black molecules are located at around $b = -0.5$ and 0.0 in the upper figure, and $b = 0.0$ and 0.5 in the lower figure, respectively, and molecules A′ and B′ are related to molecules A and B, respectively, by an inversion center. Thick and thin dotted lines indicate the S···S contacts with the lengths of <3.6 and <3.7 Å, respectively. Intermolecular overlap integrals along the molecular long axis are: $S_{AA'} = 2.0 \times 10^{-3}$, $S_{AB'} = -0.70 \times 10^{-3}$, $S_{BA'} = -0.24 \times 10^{-3}$.

(3.53–3.67 Å vs. 3.60 Å) along the molecular long axis (dotted lines in Figure 5c). Accordingly, as long as atomic contacts concern, the TTC_1-TSeF crystal has quasi-three-dimensional character.

The enhanced electric conductivity of TTC_1-TSeF ($1.3 \times 10^9\,\Omega\,cm$, $\varepsilon_a = 0.60$ eV) in Table 2 suggests the formation of a network of the heteroatomic contacts as conduction paths in the crystal, though the enhancement is not so obvious in comparison with those for $TTeC_1$-TTF ($\rho_{RT} = 6.9 \times 10^4\,\Omega\,cm$, $\varepsilon_a = 0.25$ eV)[3,4] and $TSeC_1$-TTF (Phase I, $1.0 \times 10^6\,\Omega\,cm$, 0.26 eV).[7,8,11,28a] In the case of $TTeC_1$-TTF, the molecular structure and packing pattern (Supporting Information S3) are considerably different from those of TTC_1-TSeF. Namely two methyl groups residing in diagonal positions are directed up and down from the flat plane consisting of central tetrathio-TTF moiety and two residual methyl groups, and the flat planes are arranged in parallel to form a π-column with rather large interplanar distance of 3.76 Å.[4] The most characteristic feature is that the neighboring π-columns are connected by robust and three-dimensional Te···Te atomic contacts (3.64 Å vs. 4.12 Å) affording high conductivity and μ_{TOF} (Atomic-Wire Effect).

In spite of the presence of a network of the short atomic contacts in TTC_1-TSeF, the conductivity enhancement is rather small and activation energy for conduction is considerably large. These features may be ascribed to both non-parallel packing of the π-moieties and not much shortened intermolecular heteroatomic contacts due to the small outer chalcogen atoms; sulfur.

TTC_{10}-TSeF; With large n for TYC_n-TXF, the π-segment becomes flat and two alkyl chains on one side stretch oppositely to those on the other, to form chair-like shape with dihedral angle between π-segment and alkyl chains nearly perpendicular (chair I form: TTC_n-TTF ($n = 4$–6), $TTeC_8$-TTF) or ca. 50° (chair II form: Scheme 1b, TTC_n-TTF ($n = 7$–11)).[43]

The molecular structure of TTC_{10}-TSeF (Figure 6a) exhibits chair II form with dihedral angle between $C_6Se_4S_4$ plane and outer alkyl chains of 50°. TTC_{10}-TSeF has very similar lattice parameters to those of TTC_{10}-TTF[41] and they are isostructural to each other. The π-segments of TTC_{10}-TSeF molecules show face-to-face stacking along the c axis with interplanar distance of 3.55 Å, which is longer than that in TTC_{10}-TTF by 0.06 Å (3.49 Å) (Figure 6b). There are heteroatomic contacts not only within the column (Se···Se 3.79 Å) but also between columns (Se···Se 3.67 Å, Se···S 3.69 Å) less than the sum of the van der Waals radii, as seen in Figure 6c. In the case of TTC_n-TTF ($n = 7$–11) compounds, on the other hand, short S···S contact (3.54–3.60 Å) was only observed along the intra-column direction suggesting strong one-dimensionality. Therefore, from the structural viewpoint, TTC_{10}-TSeF crystals have much higher dimensionality than TTC_n-TTF ones.

Molecular Packing. The interchain separation between the alkyl groups is a measure of the compactness of the molecular packing. The alkyl chains in hexatriacontane crystal form close packing in a trans zig-zag conformation with interchain C···C distances of 4.14–4.20 Å.[44,45] There are many short C···C distances close to or less than those in hexatriacontane within a

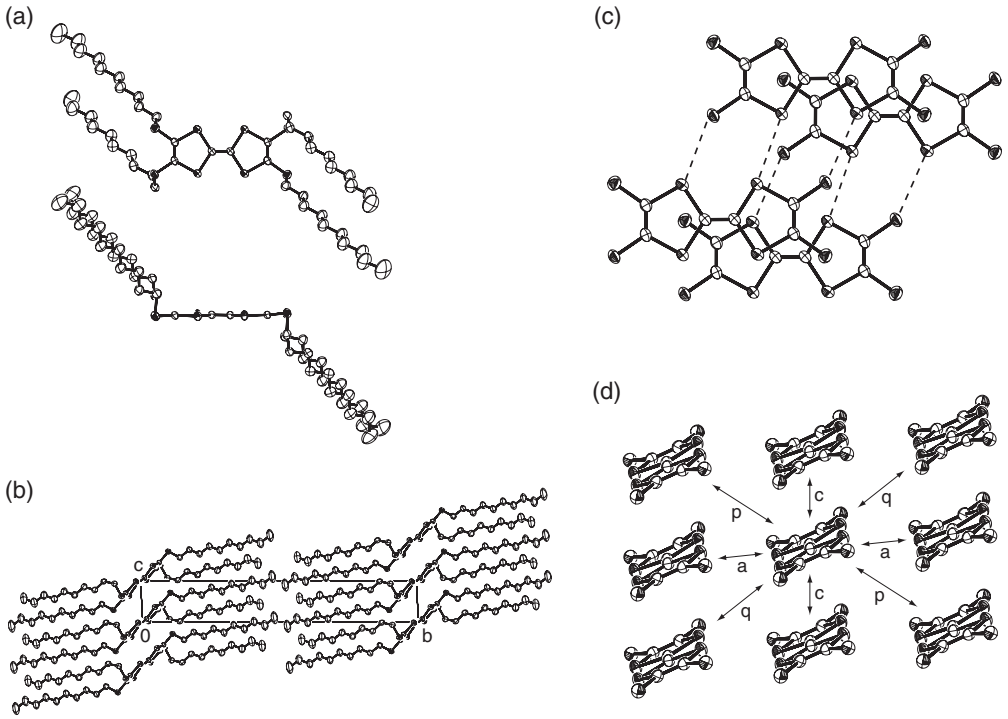

Figure 6. (a) Molecular structure and (b) crystal structure viewed along the a axis of TTC$_{10}$-TSeF. (c) Overlap pattern and side-by-side short Se···Se or Se···S contacts. (d) Intermolecular overlap integrals in a TTC$_{10}$-TSeF layer. $a = -3.4 \times 10^{-3}$, $c = 1.6 \times 10^{-3}$, $p = -1.0 \times 10^{-3}$, $q = 0.3 \times 10^{-3}$. In (c) and (d), alkyl chains are omitted for clarity.

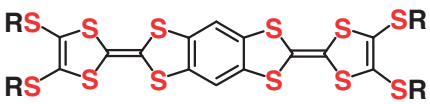

Benzene-fused bis(TTF)
R = C_nH_{2n+1}; n = 4,6,8

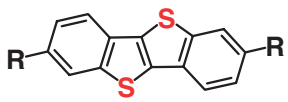

2,7-Dialkyl[1]benzothieno-[3,2-*b*]benzothiophene (C_n-BTBT)
R = C_nH_{2n+1}; n = 5-14

Scheme 4. Main molecules in this section.

molecule (Table 4A, arrow (i) in Figure 7) and between columns along the side-by-side direction (Table 4B, arrow (ii) in Figure 7), to connect the alkyl chains along the $(a + c)$ direction which corresponds to the side-by-side direction of the central $C_6X_4Y_4$ segments. There are several intermolecular C···C distances less than 4.40 Å within a column (Table 4C, arrows (iv), (v), and (vi) in Figure 7) which correspond to the van der Waals attractive ones depicted by blue arrows in Scheme 1b and are effective to fasten the π-segments. There are no short alkyl chain contacts between columns along the oblique direction (arrow (iii) in Figure 7). The short C···C distances (4.02 and 4.24 Å) were also found along the b-direction. Therefore the alkyl chains of TTC$_{10}$-TSeF form pseudo-three-dimensional close packing in the crystal. The structural analysis of TTC$_{10}$-TSeF suggests that the strong tendency of the alkyl chains to form close packing is one of the main reasons for Fastener Molecules TYC$_n$-TXF to make the π-segments squeezed and self-assembled resulting in the segregated columns of π-segments with proximate contact in an insulating media.

Perspectives of TTC$_n$-TSeF as FET Channel Materials. The Fastener Effect for TTC$_n$-TTF enhances bulk carrier mobility (μ_{TOF}, single crystal) up to 6–20 cm^2 V^{-1} s^{-1} ($n = 8$ and 10).[9] However, the field-effect mobility (μ_{FET}) of thin-film FET was found to be 10^{-5}–10^{-6} cm^2 V^{-1} s^{-1} for $n = 8$, 14, and 18.[46] The most significant difference between observed μ_{TOF} and μ_{FET} is associated with both differences in the way of carrier injection and sample crystallinity. In the form of thin-films of TTC$_n$-TTF, the carrier could be dissipated considerably after injection since the one-dimensional conduction paths are more or less deteriorated by the insulating paraffin moieties. Such a disadvantage might have manifested the low μ_{FET} of 10^{-2}–10^{-4} cm^2 V^{-1} s^{-1} on the solution processed thin-film FETs of benzene-fused bis(TTF) derivatives (Scheme 4) having one-dimensional stacking columns.[47] On the other hand, the two-dimensional feature has improved μ_{FET} for 2,7-ditridecyl[1]benzothieno[3,2-*b*]benzothiophene (C$_{13}$-BTBT) as affording moderately high μ_{FET} of 1.2–2.8 cm^2 V^{-1} s^{-1}.[48]

The calculated overlap integrals for TTC$_1$-TSeF and TTC$_{10}$-TSeF are listed in Figures 5a and 6d. The TTC$_1$-TSeF crystal

Table 4. C···C Atomic Distances of TTC_{10}-TSeF

	Distances/Å		Distances/Å
(A) Intramolecular C···C distances shorter than 4.30 Å (arrow (i) in Figure 7)			
C6A–C14A	4.075(3)	C11A–C18A	4.247(3)
C7A–C14A	4.153(3)	C11A–C19A	4.184(4)
C7A–C15A	4.218(3)	C12A–C19A	4.259(4)
C8A–C15A	4.191(3)	C12A–C20A	4.150(5)
C8A–C16A	4.133(3)	C12A–C21A	4.268(5)
C9A–C16A	4.212(3)	C13A–C20A	4.262(5)
C9A–C17A	4.189(3)	C13A–C21A	4.178(5)
C10A–C17A	4.236(3)	C13A–C22A	4.273(6)
C10A–C18A	4.153(4)		
(B) Inter-column C···C distances shorter than 4.30 Å (arrow (ii) in Figure 7)			
C4A–C14C	4.051(3)	C9A–C18C	4.197(3)
C5A–C14C	4.149(3)	C9A–C19C	4.197(4)
C5A–C15C	4.112(3)	C10A–C19C	4.202(4)
C6A–C15C	4.118(3)	C11A–C20C	4.216(4)
C6A–C16C	4.202(3)	C11A–C21C	4.264(4)
C7A–C16C	4.168(3)	C12A–C21C	4.249(5)
C7A–C17C	4.146(3)	C13A–C22C	4.249(6)
C8A–C17C	4.168(3)		
(C) Intra-column C···C distances (arrows (iv), (v), and (vi) in Figure 7)			
Arrow (iv)		Arrow (vi)	
C5A–C6B	4.274(3)	C16A–C17B	4.418(4)
C7A–C8B	4.344(3)	C18A–C19B	4.413(4)
C9A–C10B	4.400(4)	C20A–C21B	4.417(4)
		C22A–C23B	4.384(7)
Arrow (v)			
C7A–C15B	4.383(3)		

has a pseudo-three-dimensional conduction network through the overlap integrals of $p_1 = 1.6 \times 10^{-2}$ (//b), $S_{AA'} = 2.0 \times 10^{-3}$ (bc plane), and $p_2 = -6.6 \times 10^{-4}$ (//a), though the conduction path along the a axis is rather feeble. While the TTC_{10}-TSeF crystal has a two-dimensional conduction path within the ac plane with $c = 1.6 \times 10^{-3}$ and $a = -3.4 \times 10^{-3}$ and the conduction planes are separated by thick alkyl chains along the b axis.

Summarizing above, TTC_n-TSeF ($7 \leq n \leq 14$) showing Fastener Effect is a better candidate for FET channel than TTC_n-TTF analogs, because of the higher electronic dimensionality, lower on-site Coulomb repulsion which is a favorable factor for carrier conduction, lower dark conductivity to realize high off-to-on resistivity ratio, and lower donor ability to avoid the formation of charge-transfer adduct with oxygen, than those of the latter compounds, along with high solubility in conventional organic solvents (hexane, benzene, ethanol, etc.). TTC_1-TSeF makes also it an attractive candidate for FET channel; namely, low dark conductivity, low donor ability, and on-site Coulomb repulsion energy, pseudo-three-dimensional network of heteroatomic contacts, and high solubility in organic solvents.

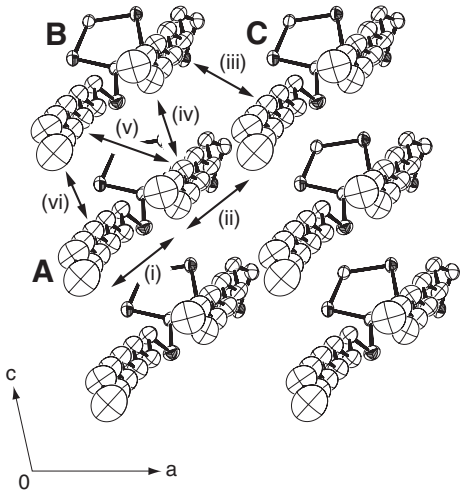

Figure 7. Trans zig-zag conformation of alkyl chains in TTC_{10}-TSeF crystal, for which only half of the molecules are depicted. For arrows, see text.

Summary

A series of TTC_n-TSeF ($n = 1$–15) were successfully prepared by a one-step reaction between dialkyl disulfide and tetralithiated TSeF. Redox potentials in 1,2-dichloroethane and optical absorption in chloroform are independent of the length of alkyl chains. TTC_n-TSeF compounds are weak electron donor molecules and characterized by small on-site Coulomb repulsion. The melting points exhibited a rapid decrease at the initial n stage, showing minimum of 22.9 °C ($n = 5$) then a gradual increase at large n likely those of TYC_n-TTF (Y = T, Se, and Te) compounds. The small n compound, TTC_1-TSeF exhibited a glassy state and two crystallization temperatures before melting similar to those of TTC_n-TTF ($n = 2$, 4, 5, and 7). For large n compound, TTC_{10}-TSeF showed a solid–solid transition just below melting like those of TYC_n-TTF (Y = T and Se) compounds with long alkyl chains. Electrical conductivity exhibited peculiar enhancement for $n = 1$ and $7 \leq n \leq 14$ owing to the presence of high-dimensional heteroatomic contacts among the π-moieties by Atomic-Wire Effect and Fastener Effect, respectively. TTC_1-TSeF has a pseudo-three-dimensional conduction network with RT resistivity of $1.3 \times 10^9\,\Omega$cm. The π-moieties of TTC_{10}-TSeF were fastened to form π-columns with interplanar distance of 3.55 Å and there are a variety of short heteroatomic contacts resulting in two-dimensional electronic structure showing resistivity of $1.5 \times 10^7\,\Omega$cm while the TYC_n-TTF derivatives showed only quasi-one-dimensional nature. The structural analysis of TTC_{10}-TSeF suggests that the strong tendency of the alkyl chains to form close packing is one of the main reasons for Fastener Molecules TYC_n-TXF to make the π-segments squeezed and self-assembled resulting in the segregated columns of the π-segments with proximate contacts. These compounds having Atomic-Wire Effect or Fastener Effect may manifest high carrier mobility, and are good candidates based on the advantageous features: low dark conductivity, low donor ability, and on-site Coulomb repulsion energy, high-dimensional π-electron structure, and high solubility in organic solvents.

Supporting Information

Detailed characterizations of dialkyl disulfides, elemental analysis, and NMR and UV–vis data of TTC_n-TSeF, crystallographic data of TTC_1-TSeF and TTC_{10}-TSeF, and molecular and crystal structures of $TTeC_1$-TTF. This material is available free of charge on the Web at: http://www.csj.jp/journals/bcsj/.

References

1 H. Inokuchi, G. Saito, P. Wu, K. Seki, T. B. Tang, T. Mori, K. Imaeda, T. Enoki, Y. Higuchi, K. Inaka, N. Yasuoka, *Chem. Lett.* **1986**, 1263.

2 K. Seki, T. B. Tang, T. Mori, W. P. Ji, G. Saito, H. Inokuchi, *J. Chem. Soc., Faraday Trans. 2* **1986**, *82*, 1067.

3 K. Imaeda, T. Enoki, Z. Shi, P. Wu, N. Okada, H. Yamochi, G. Saito, H. Inokuchi, *Bull. Chem. Soc. Jpn.* **1987**, *60*, 3163.

4 H. Inokuchi, K. Imaeda, T. Enoki, T. Mori, Y. Maruyama, G. Saito, N. Okada, H. Yamochi, K. Seki, Y. Higuchi, N. Yasuoka, *Nature* **1987**, *329*, 39.

5 H. Yamamoto, K. Seki, H. Inokuchi, G. Saito, *J. Chem. Soc., Faraday Trans. 2* **1987**, *83*, 2151.

6 P. Wang, T. Mori, C. Nakano, Y. Maruyama, H. Inokuchi, N. Iwasawa, H. Yamochi, H. Urayama, G. Saito, *Bull. Chem. Soc. Jpn.* **1988**, *61*, 3455.

7 P. Wang, T. Enoki, K. Imaeda, N. Iwasawa, H. Yamochi, H. Urayama, G. Saito, H. Inokuchi, *J. Phys. Chem.* **1989**, *93*, 5947.

8 P. Wang, T. Inabe, C. Nakano, Y. Maruyama, H. Inokuchi, N. Iwasawa, G. Saito, *Bull. Chem. Soc. Jpn.* **1989**, *62*, 2252.

9 Y. Li, C. Nakano, K. Imaeda, H. Inokuchi, Y. Maruyama, N. Iwasawa, G. Saito, *Bull. Chem. Soc. Jpn.* **1990**, *63*, 1857.

10 C. Nakano, K. Imaeda, T. Mori, Y. Maruyama, H. Inokuchi, N. Iwasawa, G. Saito, *J. Mater. Chem.* **1991**, *1*, 37.

11 C. Nakano, P. Wang, T. Mori, Y. Maruyama, H. Inokuchi, H. Yamochi, G. Saito, *Bull. Chem. Soc. Jpn.* **1991**, *64*, 3690.

12 S. Kimura, H. Kurai, T. Mori, *Tetrahedron* **2002**, *58*, 1119.

13 M. Ashizawa, S. Kimura, T. Mori, Y. Misaki, K. Tanaka, *Synth. Met.* **2004**, *141*, 307.

14 Y. Yamashita, S. Tanaka, K. Imaeda, H. Inokuchi, M. Sano, *J. Org. Chem.* **1992**, *57*, 5517.

15 K. Imaeda, Y. Yamashita, Y. Li, T. Mori, H. Inokuchi, M. Sano, *J. Mater. Chem.* **1992**, *2*, 115.

16 J. S. Zambounis, J. Mizuguchi, G. Rihs, O. Chauvet, L. Zuppiroli, *J. Appl. Phys.* **1994**, *76*, 1824.

17 M. Mas-Torrent, M. Durkut, P. Hadley, X. Ribas, C. Rovira, *J. Am. Chem. Soc.* **2004**, *126*, 984.

18 C. Rovira, J. Tarrés, J. Veciana, M. C. Rovira, J. J. Novoa, S. Yang, D. O. Cowan, E. Canadell, *Adv. Mater.* **1995**, *7*, 1023.

19 C. Nakano, T. Mori, K. Imaeda, N. Yasuoka, Y. Maruyama, H. Inokuchi, N. Iwasawa, G. Saito, *Bull. Chem. Soc. Jpn.* **1992**, *65*, 2086.

20 P. Wu, G. Saito, K. Imaeda, Z. Shi, T. Mori, T. Enoki, H. Inokuchi, *Chem. Lett.* **1986**, 441.

21 N. Okada, H. Yamochi, F. Shinozaki, K. Oshima, G. Saito, *Chem. Lett.* **1986**, 1861.

22 H. Yamochi, N. Iwasawa, H. Urayama, G. Saito, *Chem. Lett.* **1987**, 2265.

23 Z. Shi, T. Enoki, K. Imaeda, K. Seki, P. Wu, H. Inokuchi, G. Saito, *J. Phys. Chem.* **1988**, *92*, 5044.

24 J. K. Jeszka, T. Enoki, Z. Shi, K. Imaeda, H. Inokuchi, N. Iwasawa, H. Yamochi, G. Saito, *Mol. Cryst. Liq. Cryst.* **1991**, *196*, 167.

25 C. Nakano, T. Mori, K. Imaeda, N. Yasuoka, Y. Maruyama, H. Inokuchi, N. Iwasawa, G. Saito, *Bull. Chem. Soc. Jpn.* **1992**, *65*, 1878.

26 Z. Shi, K. Imaeda, C. Nakano, H. Inokuchi, T. Enoki, G. Saito, *Mol. Cryst. Liq. Cryst.* **1995**, *268*, 161.

27 T. Tanaka, T. Atake, Z. Shi, C. Nakano, T. Enoki, G. Saito, H. Inokuchi, *J. Phys. Chem. Solids* **1997**, *58*, 295.

28 a) N. Iwasawa, G. Saito, K. Imaeada, T. Mori, H. Inokuchi, *Chem. Lett.* **1987**, 2399. b) N. Iwasawa, H. Urayama, H. Yamochi, G. Saito, K. Imaeda, T. Mori, Y. Maruyama, H. Inokuchi, T. Enoki, Y. Higuchi, N. Yasuoka, *Synth. Met.* **1988**, *27*, 463.

29 R. Friend, *Nature* **1987**, *329*, 14.

30 G. M. Sheldrick, *SADABS, Program for Siemens Area Detector Absorption Correction*, University of Göttingen, Germany, **1996**.

31 G. M. Sheldrick, *SHELXS-97, Program for the Solution of Crystal Structures*, University of Göttingen, Germany, **1997**.

32 G. M. Sheldrick, *SHELXL-97, Program for the Refinement of Crystal Structures*, University of Göttingen, Germany, **1997**.

33 R. Ramakumar, Y. Tanaka, K. Yamaji, *Phys. Rev. B* **1997**, *56*, 795.

34 E. M. Engler, D. C. Green, J. Q. Chambers, *J. Chem. Soc., Chem. Commun.* **1976**, 148.

35 S. Chorbadzhiev, *God. Sofii. Univ. "Sv. Kliment Okhridski," Khim. Fak.* **1979**, *73*, 65.

36 G. Saito, *Pure Appl. Chem.* **1987**, *59*, 999.

37 a) F. Wudl, E. Aharon-Shalom, *J. Am. Chem. Soc.* **1982**, *104*, 1154. b) R. D. McCullough, G. B. Kok, K. A. Lerstrup, D. O. Cowan, *J. Am. Chem. Soc.* **1987**, *109*, 4115.

38 T. Senga, K. Kamoshida, L. A. Kushch, G. Saito, T. Inayoshi, I. Ono, *Mol. Cryst. Liq. Cryst.* **1997**, *296*, 97.

39 W. Xu, L.-M. Wang, R. A. Nieman, C. A. Angell, *J. Phys. Chem. B* **2003**, *107*, 11749.

40 C. Katayama, M. Honda, H. Kumagai, J. Tanaka, G. Saito, H. Inokuchi, *Bull. Chem. Soc. Jpn.* **1985**, *58*, 2272.

41 Y. Higuchi, K. Inaka, N. Yasuoka, private communication. TTC_2-TTF: Monoclinic, $P2_1/c$, $a = 10.220(2)$, $b = 8.759(2)$, $c = 22.950(4)$ Å, $\beta = 96.69(1)°$, $V = 2040.4(7)$ Å^3, $Z = 1$. TTC_{10}-TTF: Triclinic, $P\bar{1}$, $a = 7.850(3)$, $b = 32.960(9)$, $c = 5.115(4)$ Å, $\alpha = 92.46(3)$, $\beta = 101.16(3)$, $\gamma = 88.18(3)°$, $V = 1297(1)$ Å^3, $Z = 1$.

42 A. Bondi, *J. Phys. Chem.* **1964**, *68*, 441.

43 The definition of chair I form and chair II form in this text is different from those in Ref. 24b and the following reference: G. Saito, H. Yamochi, N. Iwasawa, H. Murofushi, T. Tachikawa, *Phosphorus, Sulfur Silicon Relat. Elem.* **1992**, *67*, 367. The definition here is a simplified one to classify based on the dihedral angle between π-segment and alkyl chains without considering the conformation of alkyl chains.

44 H. M. M. Shearer, V. Vand, *Acta Crystallogr.* **1956**, *9*, 379.

45 P. W. Teare, *Acta Crystallogr.* **1959**, *12*, 294.

46 S. Ukai, S. Igarashi, M. Nakajima, K. Marumoto, H. Ito, S. Kuroda, K. Nishimura, Y. Enomoto, G. Saito, *Colloids Surf., A* **2006**, *284–285*, 589.

47 a) X. Gao, W. Wu, Y. Liu, W. Qiu, X. Sun, G. Yu, D. Zhu, *Chem. Commun.* **2006**, 2750. b) X. Gao, W. Wu, Y. Liu, S. Jiao, W. Qiu, G. Yu, L. Wang, D. Zhu, *J. Mater. Chem.* **2007**, *17*, 736.

48 H. Ebata, T. Izawa, E. Miyazaki, K. Takimiya, M. Ikeda, H. Kuwabara, T. Yui, *J. Am. Chem. Soc.* **2007**, *129*, 15732.